07,04

# Defect structure formation in quartz single crystal at the early stages of deformation

© E.E. Damaskinskaya[1], V.L. Hilarov[1], Yu.G. Nosov[1], K.M. Podurets[2],
A.A. Kaloyan[2], D.V. Korost[3], I.A. Panteleev[4]

[1] Ioffe Institute,
St. Petersburg, Russia
[2] National Research Center „Kurchatov Institute",
Moscow, Russia
[3] Moscow State University,
Moscow, Russia
[4] Institute of Continuous Media Mechanics, Ural Branch, Russian Academy of Sciences,
Perm, Russia

E-mail: Kat.Dama@mail.ioffe.ru

Accumulation of defects in the synthetic quartz single crystal has been investigated at the early stages of deformation. Process is studied with the help of three independent nondestructive techniques, namely: acoustic emission, X-ray computed tomography and synchrotron radiation topography. It is shown that results obtained by the three techniques are consistent with each other, allow detecting the area of defect formation and, what is more important, to match acoustic emission parameters with the ones of defects. This result is of practical importance, since it makes it possible to further identify areas of fracture growth and estimate their size *in situ* only by analyzing acoustic emission data in cases where the use of other control methods is impossible.

**Keywords:** acoustic emission, X-ray computed tomography, synchrotron radiation topography (X-ray Diffraction Imaging), quartz single crystal, defects volume.

## 1. Introduction

The process of defect structure formation and development in a material under mechanical stresses has not still been fully studied. This is due to the complexity of experimental observation of defects in the bulk during deformation without violating the integrity of the object under study (sample). One of the methods to control material damage *in situ* is the recording of signals of acoustic emission (AE), which accompanies the origination and development of submicro-, micro- and macrocracks [1]. It was shown that acoustic emission in quartz occurs under high pressures, heating, and accompanies phase transformations [2–5].

A number of empirical relations between geometric parameters (length, surface area, volume) of acoustic emission (AE) signal sources and parameters of elastic wave generation (AE intensity, energy etc.) have been accumulated by now. As a rule, these relations were obtained in laboratory experiments with sample deformation either for a single cracks [6–8] or for an ensemble of surface cracks in the stress raiser vicinity [9,10].

However, for the general case of defect structure formation in the bulk material (in the absence of a macro stress raiser), we still do not have a clear understanding of the relation between the parameters of AE signals and the parameters of a signal source — a defect.

The present paper is aimed at studying the defect evolution by means of complementary techniques — acoustic emission (AE), computed microtomography (CT) and X-ray Diffraction Imaging (XDI or topography).

## 2. Sample material

We used a synthetic quartz crystal of the Z orientation grown by hydrothermal synthesis in at the All-Russian Scientific-Research Institute of Mineral Resources [11]. With this orientation, the wide crystal side faces are the pinacoid faces {0001}. The surface of such faces usually has a bumpy structure. Cylindrical samples ($d = 10$ mm, $h = 20-24$ mm) were cut out from the crystal perpendicularly to the pinacoid faces, and the sample axis is the direction $\langle 0001 \rangle$, i.e. the optical axis. The cylindrical surface was ground and polished to optical transparency. Fig. 1 shows the overall view of the test samples. Digit *1* shows the sample center where the seed is located, since in this growing method the crystal grows from both its surfaces. The two rows of dashed white dots on each sample (Fig. 1) show the seed initial surfaces decorated with defects formed in the first layers of growing quartz. These defects are
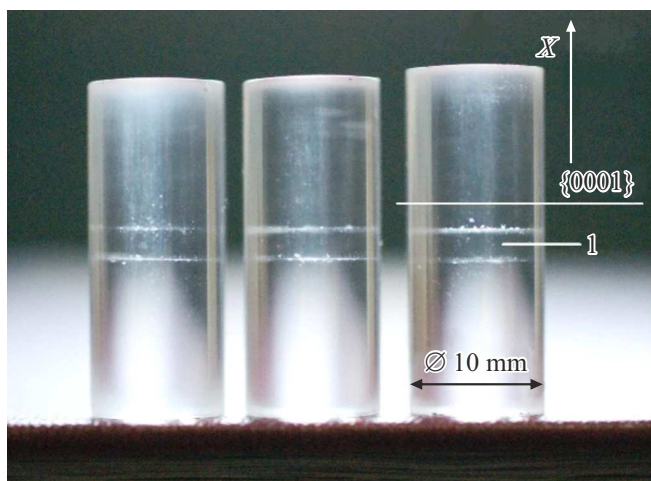
**Figure 1.** Samples of quartz single crystal.

usually gas-liquid vacuoles sized from several microns to $0.2-0.3$ mm.

Sample sizes and shape were selected so that, on the one hand, to make possible the determination of the coordinates of acoustic emission sources' hypocenters, and on the other hand — to attain the best spatial resolution during X-ray computed tomography.

## 3. Experimental procedure

The samples were subjected to uniaxial quasi-static compression with the loading rate (displacement of loading plates) of $5\,\mu$m/min using the AGX-Plus electromechanical RISC (Shimadzu, Japan, the maximum force 30 tons). Mechanical stress was applied parallel to the cylinder axis. Compression was performed to a force of 6 kN, corresponding to 0.08 from $F_{max}$ ($F_{max}$ is the breaking load determined in preliminary experiments). Then the sample was maintained under constant deformation until AE decreased to zero.

In the course of sample loading, acoustic emission signals were recorded in real time using an Amsy-5 Vallen system (Germany). Two AE105A piezoelectric converters (operating frequency range $450-1150$ kHz) were fastened in special hollow cylindrical slabs, used for direct loading of the sample. Such an arrangement of piezoelectric converters made it possible to determine the coordinates of the AE signal hypocenters with an accuracy not worse than 1.5 mm. Each acoustic emission signal was characterized by radiation time, source coordinate along the sample height, and energy. The experiment details have been described earlier, for instance, [12].

The samples' defect structure before and after mechanical tests was studied by X-ray microtomography (CT) using a SkyScan 1172 tomograph (Bruker, Belgium) equipped with a Hamamatsu 100/250 microfocus X-ray tube and a detector

(CCD-matrix of 11 Mpixel). The following scanning parameters were set: voltage 70 kV, current $129\,\mu$A, distance from source to camera (detector) 213.580 mm, distance from source to object 75.030 mm. The sample turning interval was $0.200°$, exposure time was 3770 ms, shooting duration was 24 h. Reconstruction, i.e. recalculation of the obtained projection set into a set of density flows, reflecting the internal sample structure, was performed using the NRecon software from SkyScan Company. All data was reconstructed with equal HU brightness parameters (from $-650$ to 2200), which allows for comparing the results of different shootings, and provides an objective check of the results.

The chosen sample size made it possible to attain the computer tomography spatial resolution of $\sim 3\,\mu$m, which is the maximum possible value for the given sample size, taking into account the physical principles of tomography, the design features of the X-ray tube and the tomograph camera [13].

Sample tomography prior to mechanical tests has revealed defects remaining from the seed surface. Three-dimensional visualization of the sample structure near the seed is shown in Fig. 2. It is seen that the defects are randomly located inside the sample in the region with coordinates $11-14$ mm along the height. The seed was located exactly in this region. No crack-type defects (discontinuities) were found outside the seed plane.

Tomography can only reveal defects characterizing by variation of material electron density. Such defects can include voids and inclusions of a different phase. However, crystals can have defects that do not affect material density but generate internal stresses, which may affect the breakdown process. Such stress fields are generated by crystalline structure defects and their clusters. X-ray topography makes it possible to obtain an image of long-range deformation fields in the form of diffracted beam intensity change (due to extinction contrast) [14].

Papers [15–18] deal with quartz structure defects in order to reveal their influence on functional properties of optical and semiconductor devices.
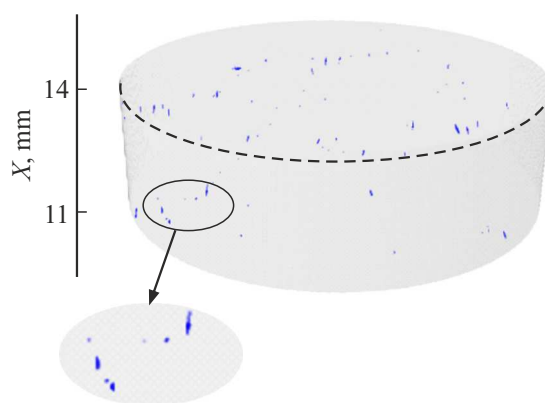


**Figure 2.** Three-dimensional visualization of initial defects (blue objects).

This paper is dedicated to a search for a correlation between the presence of crystalline structure defects and breakdown of quartz samples under a mechanical load, i.e. the formation and development of a main crack.

Topographic research was carried out at the „Mediana" station of the Kurchatov specialized synchrotron radiation source „KISI-Kurchatov". Images (topograms) were recorded using a two-axis detector based on a CCD matrix sized $4008 \times 2672$, a GdOS:Tb, scintillator with the pixel size of $8.9\,\mu$m. Images were processed using the ImageJ program [19].

In case of white beam topography, the quartz sample was placed horizontally in the symmetrical geometry „in the clear" with the horizontal diffraction plane, reflection at a Bragg angle of $\approx 12°$ was recorded by a detector located 30 cm away from the sample. The beam was limited by a vertical slit $300\,\mu$m wide, while a topogram was a projection of the sample bulk through which the beam passes (a sectional topogram).

A vertical diffraction plane was used in case of topography on a monochromatic beam. A monochromator for beam expansion was a plane silicon crystal with a surface plane deflecting from $(100)$ to $7°$, reflection $(511)$ (accordingly, the angle between the surface and the reflecting plane is $9°$), $\lambda = 0.56$ Å. Reflection asymmetry factor $b = 0.1$, beam divergence after the monochromator is estimated at $0.2''$. Shooting consisted in the making of a series of images with sample turning with the interval of $0.6''$. Shooting time for one image was 10 s. The sample was placed horizontally, so that the detector might record the image of the whole crystal; thus, deformation distribution over the entire crystal volume can be observed by means of X-ray topography. However, different crystal areas did not reflect simultaneously due to dispersion. In this case, an image of the entire crystal is obtained by plotting a map of distribution of the peak intensity values (on the peak of the diffraction reflection curve) for the whole array of topograms obtained with different angular positions of the crystal [20]. A topogram array can be also used to make a map of distribution of crystal swing curve width, being a characteristic of its perfection [21].

## 4. Results and discussion

Fig. 3 shows the time dependences of deformation and AE activity (number of signals per unit time). During activity calculation, the whole set of events was broken down into intervals of equal time (50 s in this case), and then the number of events in each was determined. It can be seen that activity increases in the period of deformation increase. Then, deformation being constant, activity decreases and its values remain low (signal units).

The distribution of AE signal hypocenters along the sample height is shown in Fig. 4. It can be seen that the largest number of sources (in $7-10$ times larger than in other regions) was recorded in the region of $16-20$ mm.

This result makes it possible to assume that the fastest defect formation occurs exactly in this region.

According to the data given in Section 3 above, this region contains no seed-related defects. We can assume that the initial defects in this case are not stress raisers and crack originators. Indeed, the tomography of the loaded sample confirms this assumption. Fig. 5 shows three-dimensional visualization of the formed crack $(a)$ and examples of tomographic slices $(b, c)$ parallel to the cylinder base. It can be seen that the crack (the black line in Fig. $5, a$) formed outside the initial defects (the red objects in Fig. $5, b$). A comparison of the tomographic slices before and after loading makes it possible to state that initial defects under this loading level did not experience any changes, i.e. there is neither intergrowth nor closure of defects.
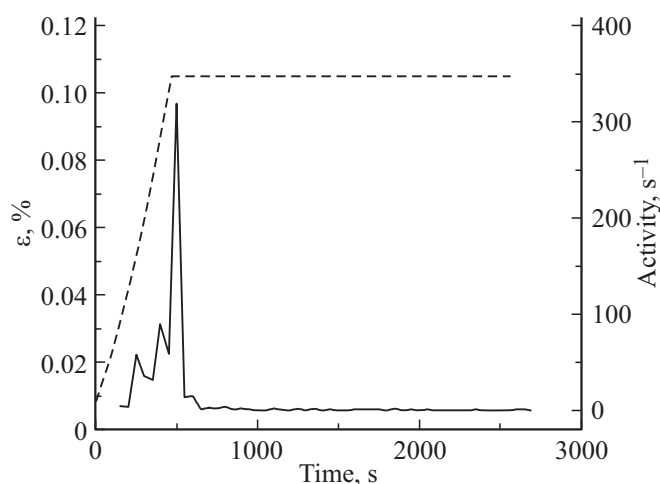


**Figure 3.** Change of deformation (dashed line) and AE activity (solid line) during the experiment.
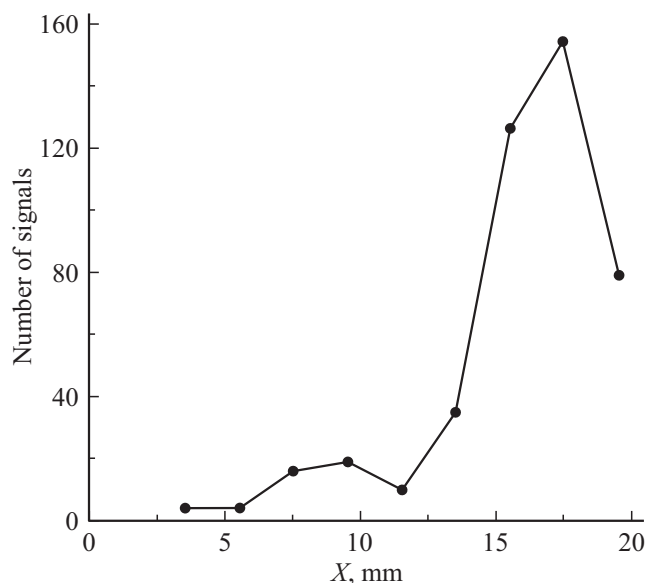


**Figure 4.** Distribution of AE signals by the coordinate (along the sample height).
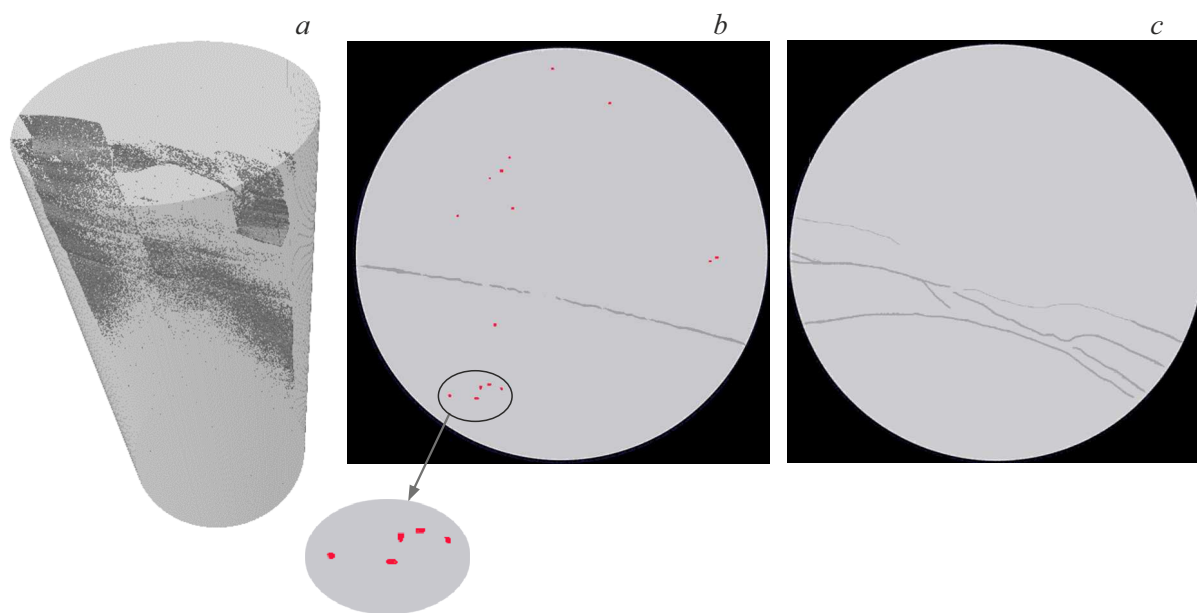
**Figure 5.** Three-dimensional visualization of the defect structure according to the data of X-ray tomography using CTan and CTvol specialized software (*a*), and examples of tomographic slices: *b* — slice from the region near the seed — the initial defects are red, the crack is black; *c* — slice from the region away from the seed with the most branched crack (black lines).

Fig. 6 shows a change of defect volume in layers 2 mm high, determined on the basis of the CT data using the CTan software package. Mean energy ($E_{\mathrm{mean}}$) of AE signals, whose hypocenters are in the given layer, was also calculated for each layer. The largest defect volume was recorded in the region of $16-20$ mm. In this region the crack has a branched structure, which is demonstrated by the tomographic slices (Fig. 5, *c*).

A comparison of the distributions of defect volume and mean energy of AE signals along the sample shows that the defect volume increase correlates with energy liberation increase. A similar result was obtained earlier [22] when
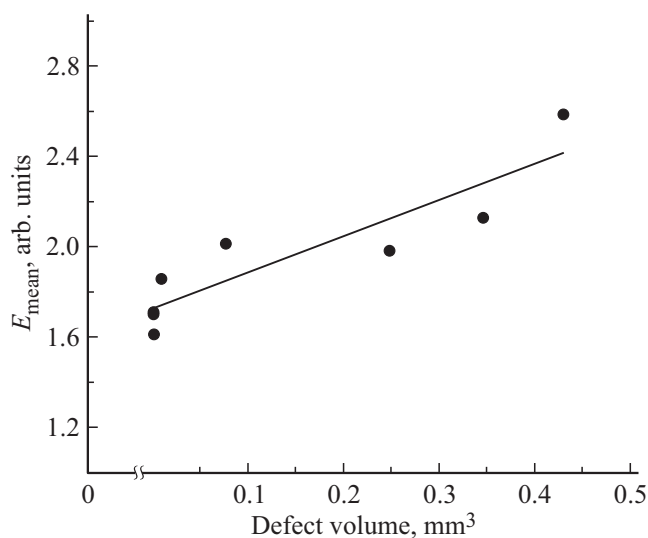


**Figure 7.** Dependence of average energy of AE signals on defect volume.



**Figure 6.** Change of mean energy of AE signals (gray curve *1*) and defect volume (red curve *2*) by the coordinate (along the sample height).

studying defect accumulation in natural heterogeneous materials. This makes it possible to speak of generality of the results and their independence from a particular material.

Moreover, a correlation between the mean energy of AE signals and defect volume was established (Fig. 7). The dependence is approximated by a linear function ($R^2 = 0.89$). This result allows for subsequent estimation of the volume of formed defects according to the parameters of AE signals.
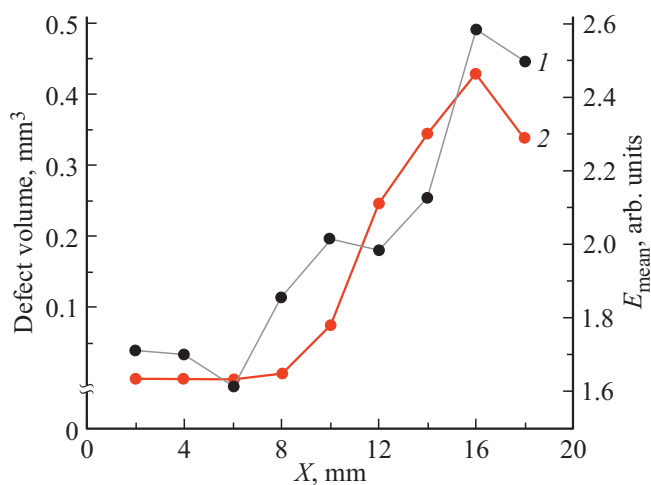
X-ray topography showed that the main „motive" of a defect structure is the presence of linear formations in the form of wavy fibers spanning the sample length, i.e. in the crystal growth direction (Fig. 8, 9). These formations in the sectional topograms have the form of a dash the width of which depends on slit width. The topograms in the monochromatic beam also show a fibrous structure,
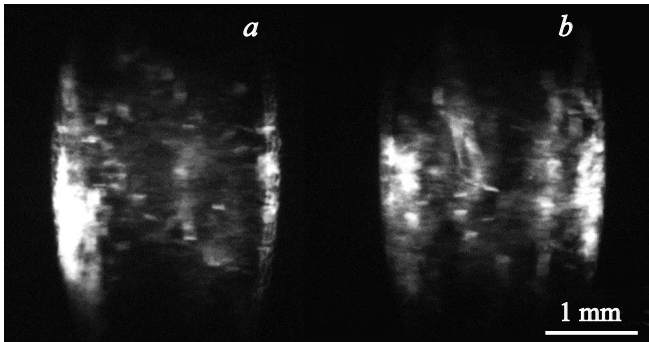


**Figure 8.** Two sectional topograms $(a, b)$ of the quartz crystal obtained with the crystal shift of 1 cm.
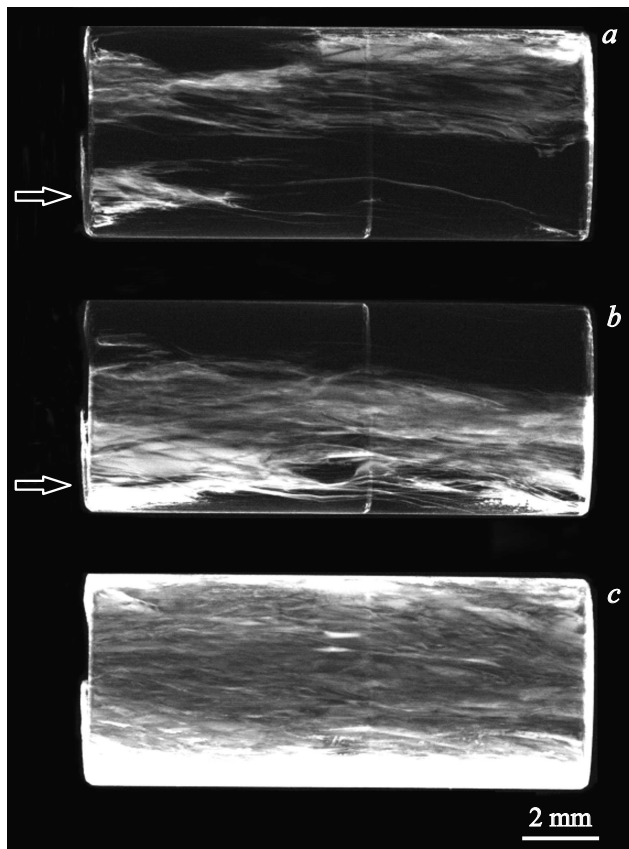


**Figure 9.** Two topograms of the quartz crystal taken before mechanical loading $(a, b)$, obtained with the angular interval of $9.4''$, and map of the maximum intensity values $(c)$. A boundary of simultaneous reflection is observed in the image middle. The arrow shows the region of increased defect density.
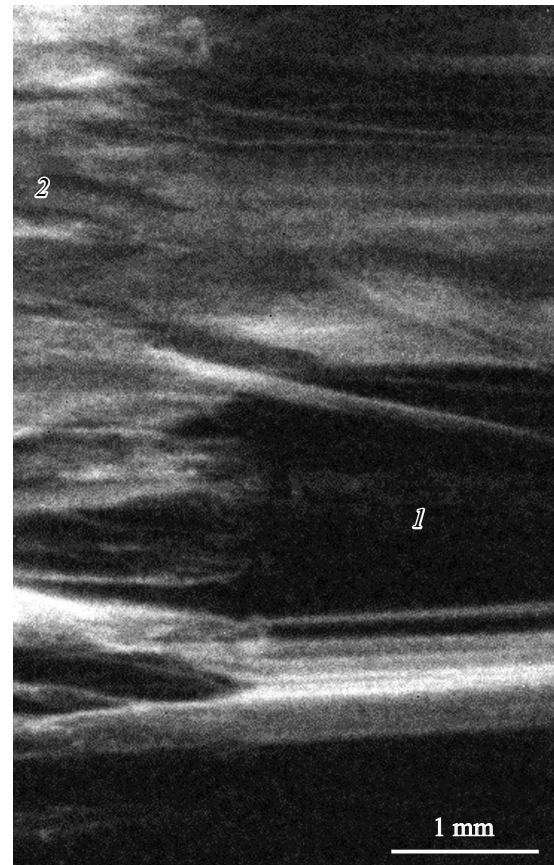
**Figure 10.** Crystal topogram near the interface of seed $(1)$ and host crystal $(2)$.

where the fibers do not represent individual linear defects (dislocations), since their ruptures are observed in many cases, which is not typical for dislocations.

Elementary defects, such as dislocations, small-angle boundaries etc. are not revealed on the topograms. The observed imperfection are not discontinuities as well. The feed plane can be seen in the topograms; fiber density in the seed is smaller than in the remaining crystal bulk. Some fibrous formations exist only outside the seed, some yield a brighter image outside the seed as compared to the image inside the seed (Fig. 10). It can be assumed that the fibrous structure reflects defect clusters, mainly dislocations, density of which is permanent along the fiber and changes considerably in the transverse direction. The crystal has a region with an increased density of fibrous formations as compared to the average density in the crystal. This region is shown by an arrow in the topograms in Fig. 9, $a$ and $b$.

Quartz crystal topograms after a mechanical action were taken. An analysis of the AE and CT data showed that the most well-developed crack (the largest defect volume) formed in the region with the coordinates of $16-20$ mm. An increased intensity is observed on the topograms (Fig. 11) in the same space region.

The map of swing curve widths obtained from the sequence of topograms at different angles also shows
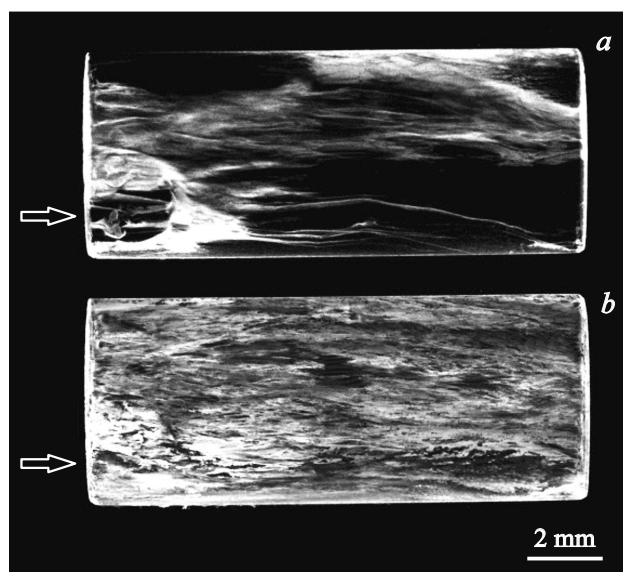
**Figure 11.** Quartz crystal topogram taken after mechanical loading (*a*), and map of swing curve width values (*b*). The arrow shows the breakdown region.

that in the same crystal region there is an increase of width $(15-20'')$ as compared to the typical value for an undamaged crystal $(3-5'')$. The location of the breakdown region in the crystal corresponds to the location of the region found in the topograms taken before mechanical action, where density of fibrous formations was increased (Fig. 9, *a* and *b*).

Thus, diffraction topography made it possible to reveal a region of increased deformations in the initial sample. The fastest crack formation took place exactly in this region after mechanical actions, which is confirmed by the computed tomography results.

It should be noted that the experimentally observed topographic pattern of fibers in the crystal bulk matches the frequently described [11,23] pattern of quartz structural defects — knots caused by clusters of grown-in dislocations. Dislocations may grow both from the seed and form on particles of an impurity captured from the solution. In the course of crystal growth, dislocations gather into „bundle" and „walls" that give rise to a knotty (fibrous) structure, i.e. what is termed „blockiness" for other crystals. The considerable disorientation of individual regions of knotty (fibrous) crystals makes it possible to see these blocks in X-ray topograms.

Since the seed is cut out from a crystal with a small number of dislocations (or from a dislocation-free one), then, as our experiments showed, the seed contains no or few knots (fibers).

Thus, the observed crack formation in the quartz crystal in places of increased knot density (fibrous formations) makes it possible to conclude that the primary structural defect, which causes crack formation under loading, is „rope-shaped" dislocation clusters along knot boundaries.

## 5. Conclusion

We studied the defect accumulation in a synthetic quartz single crystal under uniaxial compression at early deformation stages. Simultaneous use of three independent non-destructive techniques — acoustic emission, X-ray computed tomography, synchrotron radiation topography — has provided more complete information about breakdown development.

An analysis of the X-ray computed tomography data showed that a main crack starts forming at rather small stresses. It was established that a crack does not affect the initial defects. A satisfactory correlation between the volume of formed defects and average energy of AE signals, recorded during their formation, is shown.

The synchrotron radiation topography showed that a region of increased deformations can be distinguished in the sample not exposed to mechanical action. X-ray computed tomography revealed that the fastest crack formation occurred exactly in this region after load application.

It should be noted that an analysis of AE signal parameters also makes it possible to distinguish the same space region: an increased energy liberation and AE activity are observed here.

Thus,

— diffraction topography revealed a region of increased internal deformations in the initial crystal;

— computed tomography visualized the cracks that formed after load application and provided the data about defect spatial, sizes and volume;

— analysis of the parameters of acoustic emission signals made it possible to distinguish a spare region of the sample where defect formation was the fastest.

It was demonstrated that the results obtained with the help of the three methods are consistent and make it possible to reveal the region of the fastest defect formation in the sample bulk and, what is particularly important, to compare the parameters of AE signals with defect parameters.

This result has applied (practical) significance, since it allows for subsequent detection of breakdown regions and estimating their sizes *in situ* only on the basis of an analysis of acoustic emission data when other inspection methods cannot be used (for instance, during operation of industrial facilities).

### Conflict of interest

The authors declare that they have no conflict of interest.

### References

[1] X. Lei, S. Ma. Earthquake Sci. **27**, *6*, 627 (2014).

[2] A. Schmidt-Mumm. Phys. Chem. Minerals **17**, 545 (1991).

[3] P.W.J. Glover, P. Baud, M. Darot, P.G. Meredith, S.A. Boon, M. LeRavalec, S. Zoussi, T. Reuschlé. Int'l J. Geophys. **120**, *3*, 775 (1995).

[4] J. Gasc, A. Schubnel, F. Brunet, S. Guillon, H.-J. Mueller, C. Lathe. Phys. Earth. Planetary Interiors **189**, *3−4*, 121 (2011).

[5] V.I. Vettegren, V.S. Kuksenko, P.I. Shcherbakov. Tech. Phys. **56**, *4*, 577 (2011).

[6] K. Peng, S. Shi, Q. Zou, J. Mou, J. Yu, Y. Zhang, Y. Cheng. Energy Sci. Eng. **8**, *9*, 3117 (2020).

[7] S.G. Shah, J.M. Chandra Kishen. Eng. Fracture Mech. **87**, *1*, 36 (2012).

[8] S. Yuyama, Z.-W. Li, M. Yoshizawa, T. Tomokiyo, T. Uomoto. NDT & E Int'l, **34**, *6*, 381 (2001).

[9] Y. Seo, Y.R. Kim. KSCE J. Civil Eng. **12**, *4*, 237 (2008).

[10] J. Zhang. Hindawi. Shock Vibration.2018, Article ID 3057628, (2018).

[11] Sintez materialov / Ed. by B.A. Dorogovin. 2-nd ed. VNIISIMS (2000). Vol. 1. 642 p. (in Russian)

[12] E.E. Damaskinskaya, V.L. Gilyarov, I.A. Panteleyev, D.R. Gafurova, D.I. Frolov. FTT **60**, *9*, 1775 (2018) (in Russian).

[13] T. Toth, R. Hudak. Acta Mech. Slovaca **17**, *4*, 40 (2013).

[14] I.L. Shul'pina, I.A. Prokhorov. Crystallogr. Rep. **57**, 661 (2012).

[15] A.R. Lang. Nature **220**, 652 (1968).

[16] L.I. Tsinober, V.E. Khadzhi, L.A. Gordienko, L.T. Litvin. In: Rost kristallov. Nauka, M. (1977). Vol. 12. P. 75 (in Russian).

[17] V. Lerche, P. Dornfelder, J. Hartwig. Phys. Status Solidi A **128**, *2*, 269 (1991).

[18] Y. Epelboin, A. Authier. Acta Crystallogr. A **39**, 767 (1983).

[19] C.A. Schneider, W.S. Rasband, K.W. Eliceiri. Nature Meth. **9**, *7*, 671 (2012).

[20] A.A. Kaloyan, K.M. Podurets, I.A. Prokhorov, E.S. Kovalenko, I.Zh. Bezbakh, A.O. Okunev, A.I. Gribenyukov, G.A. Verozubova. Crystal Res. Technol. **53**, *11*, 1800154 (2018).

[21] D. Lübbert, T. Baumbach, J. Härtwig, E. Boller, E. Pernot. Nucl. Instrum. Meth. Phys. Res. B **160**, *4*, 521 (2000).

[22] E.E. Damaskinskaya, I.A. Panteleyev, D.V. Korost, K.A. Damaskinsky. FTT **63**, *1*, 103 (2021) (in Russian).

[23] G.V. Kleshchev, I.V. Kabanovitch, L.N. Cherny. Dokl. AN SSSR **174**, *3*, 585 (1967) (in Russian).